Doppler Effects of Wind Turbines' Rotating Blades On The Error Performance of Direct-Sequence/Spread-Spectrum Communications System

Ahmet Faruk COŞKUN, Osman KARABAYIR, Hüseyin Avni SERİM

TÜBİTAK-BİLGEM, Kocaeli, TURKEY
{ahmet.coskun,osman.karabayir,huseyin.serim}@tubitak.gov.tr

Abstract

The main objective of this paper is to examine the deterioration effects of the Doppler frequency-shift phenomena on the performance of direct-sequence (DS)/spread-spectrum (SS) communications systems caused by the wind turbines' rotating blades. By performing Monte Carlo simulations through the entire rotation period of the blades and employing numerical integration over the entire length of the blades, the variation of the bit/symbol error rates of DS/SS systems employing different modulation signals are investigated. In order to provide many useful insights on the assessment of the performance degradation caused by the Doppler phenomena, this paper exposes miscellaneous numerical results related to different operating configurations and settlings.

1. Introduction

Throughout the world, wind farms have been attracting great attention since it is one of the most environmentally friendly and efficient way of producing energy. Also, it is expected to be prominent among other energy production methods for its offering of low installation and operating costs and no atmospheric pollution [1]. However, the increase on wind energy investments raises the concerns about the deteriorating effects of wind turbines (WTs) and wind farms (WFs) on the performance of electronic systems. The investigation of the performance degradation of the military surveillance systems, military or civil navigation and communications systems, and discovering the potential techniques for mitigation (if possible) are of great importance especially from the system designers' point of view. The literature include many research efforts focused on the deteriorating effects of WTs on the performance of two-way propagating (e.g., radar) systems via several computation methods such as Physical Optics, Shooting and Bouncing Rays and Parabolic Equation. By especially examining the scattering and shadowing effects of WTs on the received power of radar signals, researches have provided perspectives to assess the degradation caused by WTs. The researches presented in [2-7] have shown that the presence of WTs can cause degradations on radar systems' performances depending on near- and far-field scattering effects. Besides, the effects of the Doppler frequency shift caused by the rotating blades of the WTs have been investigated in [8] by performing a set of measurements on scanning weather radars. These experimental results have exhibit that the Doppler spectrum caused by WTs might degrade the detection performance of existing weather signals and might give rise to false plots (i.e., ghost weather signals). Similar to the two-way propagating case, the related literature have introduced some work about one-way propagating systems consisting of military or civilian navigation systems (e.g., VHF Omnidirectional Radio (VOR) [9], Global Positioning System (GPS) [10]) and communications systems (e.g., radiocommunication links [11, 12], analog TV [13] and digital video broadcasting (DVB) systems [14]). Since the analytical nature of the Doppler frequency shifted time-domain signal representation is hard to investigate, a great portion of the previous work on this phenomena are based on scaled-model or field measurements [11-15].

The effect of Doppler frequency-shifted scattering signals on the bearing estimation performance of VOR systems is investigated in [9] by considering a simple multipath model with providing no time-dependent variations about the WT rotation dynamics and the scattering signal contribution. Also, the possible variation of the performance metrics due to the yaw angle of the investigated WT, the settlings of the radio source, the scatterer and the VOR receiver (that would result in variations in the free space loss of the direct and the indirect signals evaluated) is out of the consideration of [9]. The work presented in [10] (which also constitutes many of the mathematical and motivational base of our paper) provides a time-domain signal-based approach on a GPS satellite-helicopter link by evaluating the effects of Doppler frequency shifts caused by the rotational movement of helicopter blades. The authors have examined the Doppler frequency shift phenomena for a DS/SS communications system application by constructing a simplified signal reception case. Although the baseline presented by [10] has novelties about the derivation of the received time-domain signal, it has neglected many important points about the Doppler frequency shifted scattering model. The derivations and performance results are approximately obtained and valid under many limitations about the settlings of the transmitter, the receiver and the scatterer. However, the previous work given in [11-15] has shown the deteriorating effect of Doppler spectrum variation on the performance of communications systems by performing measurements, they lack to put forth an analytical and/or emprical scattering model and to provide a detailed reasoning base due to the operating parameters and settlings of the electronic terminals and the WT. This paper, by adapting and revising the scattering model given in [10] to a bi-static scattering scenario as depicted in Fig. 1 and Fig. 2, and by also reconsidering some approximated metrics accurately, provides a simplified but useful perspective for the performance degradation of DS/SS signals due to Doppler frequency shifted multipaths. Note that, the presented performance analysis not only consider the path-loss variation (different than [10]), but also paves the way for extending the investigated scattering model as to consider other transmission factors such as antenna pattern gains and propagation factor variation, and for the accurate evaluation of the scattering loss based on a bi-static scattering approach. In this paper, the signaling technique that has been preferred to be inves-

tigated is DS/SS for its wide usage in many civilian and military power-efficient applications. DS/SS signals has been employed in navigation systems such as GPS, Galileo (Search and Rescue Mode at 406.0 MHz - 406.1 MHz Band), GLONASS, and cordless phones (at 900 MHz, 2.4 GHz and 5.8 GHz), IEEE 802.11b 2.4 GHz Wi-Fi and Automatic Meter Reading (AMR) systems at 460 MHz ISM Band. Some of the benefits of these signals are their resistant structure to intended or unintended jamming signals, their ability to share a single channel among multiple users and to provide a reduced signal-to-background noise ratio level that brings along with a low probability of interception.

The remainder of this paper is organized as follows. In Section II, we present the investigated scattering problem, and the telecommunications system model, and briefly define useful terms related to the Doppler scattering efects. The average BER/SER performance results that are obtained via Monte Carlo simulations are exposed in Section III, and miscallenous numerical results are presented. Finally, Section IV draws conclusions about the numerical results related to the WT scattering problem.

2. Signal Model And Problem Definitions

The investigated scattering scenario is depicted in Fig. 1 (3-D view) and Fig. 2 (2-D projection on X-Y plane).

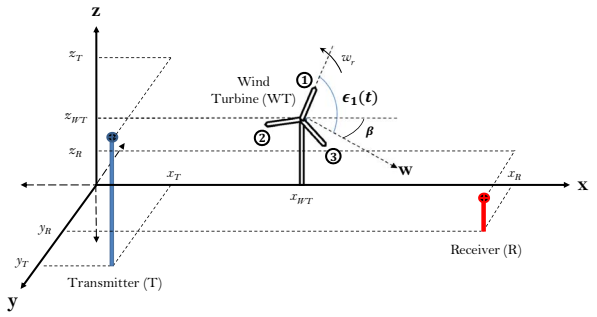

Figure 1. Three Dimensional Schematic Representation: Settlings of the transmitter, receiver and wind turbine

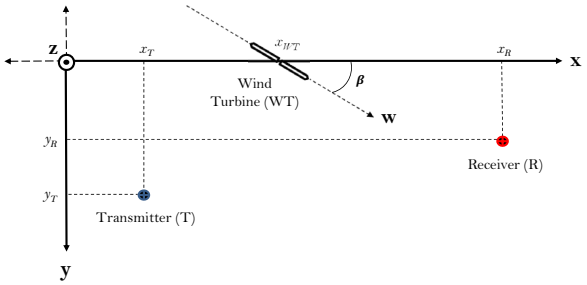

Figure 2. Two Dimensional Schematic Representation on X-Y Plane: Settlings of the transmitter, receiver and wind turbine

As seen in the DS/SS transmitter and receiver structure depicted in Fig. 3, the transmitter system $\mathbf{T}$ employs M-PSK mapping and carrier modulation followed by pseudo-noise (PN) code spreading of the data bits. As predicted, the receiver $\mathbf{R}$ employs the same procedure in the reversed order to demodulate and despread the received signal waveforms.

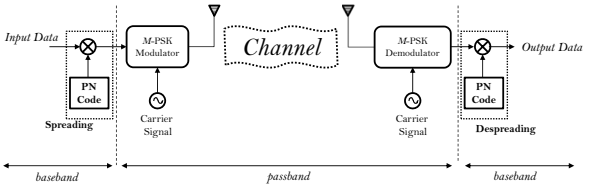

Figure 3. Block Diagram of DS/SS Transmitter and Receiver

After despreading the demodulated signal waveform, the decision metric is shown in [10, 16] to be obtained as

$$z(n) = b(n) + b(n)\zeta(n) + \eta(n), \tag{1}$$

for the nth transmitted data symbol (i.e., b(n)) where $n = 1, 2, \ldots, N$, and N is the total number of data symbols transmitted. Here, $\zeta(n)$ and $\eta(n)$ denotes the samples of the time-varying scattering component contribution (SCC) $\zeta(t)$ and the additive white Gaussian noise (AWGN) process $\eta(t)$ at the receiver after despreading at time instants $t = nT_s$ where T_s is the symbol period. By applying the decision metric given in (1) would simply result in the estimate of the transmitted data symbol. In [10], the SCC in (1) is shown to be approximated as

$$\zeta(t) = \mathcal{P}_{\mathcal{S}}(t)\mathcal{C}_{\mathcal{S}} \sum_{m=1}^{M_b} \int_0^{L_b} \left(1 - \frac{|\tau_m(t)|}{T_c}\right) e^{j\Psi_m(t)} dr, \tag{2}$$

where $\mathcal{P}_{\mathcal{S}}(t)$, $\mathcal{C}_{\mathcal{S}}$, $\tau_m(t) = \frac{1}{c}(L_1(t) + L_2(t) - L_0)$ and $\Psi_m(t)$ are respectively the relative path-loss factor of the scattered signal with respect to the direct path, the scattering coefficient, the time delay and the Doppler phase term of the scattered signal from the scatterer point ($\mathbf{S}$) on the mth blade at distance r to the rotation center, c is the speed of light, M_b is the number of rotating blades, L_b is the blade length and T_c is the duration of the chip waveform [10, 16]. L_0, $L_1(t)$ and $L_2(t)$ are respectively the distances between $\mathbf{T}$ and $\mathbf{R}$, $\mathbf{T}$ and $\mathbf{S}$, and $\mathbf{S}$ and $\mathbf{R}$. By using the cartesian coordinates of the transmitter $\mathbf{T} = (T_x\ T_y\ T_z)$, the receiver $\mathbf{R} = (R_x\ R_y\ R_z)$ and the scatterer point $\mathbf{S}(t) = (S_x(t)\ S_y(t)\ S_z(t))$, the Euclidean distances can be obtained as $L_0 = ||\mathbf{T} - \mathbf{R}||$, $L_1(t) = ||\mathbf{T} - \mathbf{S}(t)||$ and $L_2(t) = ||\mathbf{S}(t) - \mathbf{R}||$ where $||\cdot||$ represents the vector norm operator. Here, $\mathcal{P}_{\mathcal{S}}$ is simply the relative path loss factor normalized to the path loss factor of the direct path and defined as

$$\mathcal{P}_{\mathcal{S}}(t) = \frac{1}{\sqrt{4\pi}} \frac{L_0}{L_1(t)L_2(t)}. \tag{3}$$

The phase term related to the Doppler frequency shifted multipaths can be written as

$$\Psi_m(t) = -\frac{2\pi}{\lambda}(L_1(t) + L_2(t) - L_0)$$
$$-\frac{2\pi r}{\lambda}(\mathbf{v}_m(t)\cdot\mathbf{l_1}(t)) + (\mathbf{v}_m(t)\cdot\mathbf{l_2}(t)) \tag{4}$$

in terms of the unit-norm vectors $\mathbf{l_1}(t)$ and $\mathbf{l_2}(t)$ along the direction from $\mathbf{T}$ to $\mathbf{S}$, and $\mathbf{S}$ to $\mathbf{R}$, respectively and the unit-norm vector $\mathbf{v}_m(t)$ corresponding to the rotational movement of the mth blade. The time-varying unit-norm vector identities can be derived in terms of the time-varying distance metrics, the rotational angle of each blade and the distance r. The

rotational angle of each blade can be expressed as $\epsilon_m(t) = \epsilon_0 + \frac{2\pi(m-1)}{M_b} + w_r t$, $m = 1, 2, \ldots, M_b$, where w_r is the rotation frequency of WT and ϵ_0 denotes the rotation offset angle of the first blade ($m = 1$) with respect to $\mathbf{w}$-axis that is on the plane of rotation and parallel to X - Y plane. By using the rotation angles of each blade, the unit-norm vector representing the rotational motion would be obtained as

$$\mathbf{v}_m(t) = \mathbf{z}\cos(\epsilon_m(t)) - \mathbf{w}\sin(\epsilon_m(t)), \quad (5)$$

where $\mathbf{z}$ and $\mathbf{w}$ represents the unit-norm vectors along the axes z and w. Considering the fact that the unit-norm vector $\mathbf{w}$ can be decomposed into the unit vectors along the axes x and y as $\mathbf{w} = \mathbf{x}\cos(\beta) - \mathbf{y}\sin(\beta)$, (4) can be rewritten in terms of the cartesian coordinates as

$$\mathbf{v}_m(t) = -\mathbf{x}\cos(\beta)\sin(\epsilon_m(t)) + \mathbf{x}\sin(\beta)\sin(\epsilon_m(t)) + \mathbf{z}\cos(\epsilon_m(t)), \quad (6)$$

Note that, however, the reference [10] has provided an approximate expression for the Doppler phase term by making it valid only for $T_y = 0$ (i.e., T lies on the X - Z plane), (4) is exactly valid for all cases of settling configurations of $\mathbf{T}$, $\mathbf{R}$ and WT.

By substituting the delay of the scattering signal delay $\tau_m(t) = \frac{1}{c}(L_1(t) + L_2(t) - L_0)$ the Doppler phase term given in (4) into (1), and performing the numerical integration over the extend of the WT blade, one can easily obtain the SCC. Considering the SCC on the received signal, it would be useful to examine the bit/symbol error rate (BER/SER) performance of communications systems employing DS/SS in a time-varying multipath environment. In the following section, we have presented the computer simulation results for miscellaneous system parameters, modulation levels and point of views, that have been obtained via the Monte Carlo method.

3. Numerical Results

In order to examine the deteriorating effect of Doppler frequency shifted multipath environment yielded by the presence of WT on the performance of DS/SS communications systems, we present some numerical results in this section consisting of Monte Carlo simulation results of miscellaneous operating parameters and settling conditions for the transmitter, the receiver and the WT. The basic parameter set that are used in the computer simulations are listed below in Table 1.

Table 1. Basic Simulation Parameters

Parameter	Notation	Value	Unit
Center frequency-1	$f_{c,1}$	400	MHz
Center frequency-2	$f_{c,2}$	1000	MHz
Transmitter Tower Height	T_{TH}	15	m
Receiver Tower Height	R_{TH}	15	m
WT Hub Height	WT_{HH}	90	m
Number of WT Blades	M_b	3	-
WT Blade Length	L_b	40	m
Rotation Speed of WT	$w_r/2\pi$	0.25	radians/s
Offset Angle of 1st Blade	ϵ_0	$\pi/18$	radians
Symbol Duration	T_s	10^{-5}	s
Chip Duration	T_c	10^{-7}	s

For the performance results given in Figures 4-7, the settlings (in cartesian coordinates as depicted in Figures 1 and 2) of the transmitter and receiver terminals and the WT hub have been set as $\mathbf{T} = (1000\ -500\ 1215)$, $\mathbf{R} = (21000\ -500\ 615)$ and $\mathbf{WT} = (21000\ 1500\ 540)$, respectively.

The average BER/SER results are obtained and averaged over Monte Carlo simulations that have been run for multiple repetations of the one-third of the WT rotation period. Based on the number of WT blades (i.e., $M_b = 3$), the transmission/reception problem has a 120°-symmetrical characteristics. By considering the value of the rotation speed of the WT given in Table 1, the one-third duration of the investigated time interval is $[0 - \frac{4}{3}]$ s. Note that, however we have provided the performance results as accurate as possible, the average BER results own a increased accuracy trend by the increasing number of Monte Carlo runs.

In Figure 4, the average BER performance variation of BPSK signals are depicted due to varying values of the average received SNR, for the center frequency of $f_{c,1} = 400$ MHz, two different scattering coefficients $\mathcal{C}_\mathcal{S} \in \{3, 15\}$ dB and four different values of the WT yaw angle $\beta \in \{0^\circ, 40^\circ, 90^\circ, 140^\circ\}$. The average BER performance of DS/SS-BPSK signals is seen to follow a degrading tendency for the increasing values of the scattering coefficient ($\mathcal{C}_\mathcal{S}$) since any increase in the value of this parameter directly enlarges the scattering component contribution (i.e., middle term given in (1)). Also, for a fixed value of $\mathcal{C}_\mathcal{S}$, the average BER performance differs due to varying values of the WT orientation angle β. One can easily see that the average performance of the investigated communications system due to varying values of β is sorted in degrading order as for $\beta = 40^\circ$, $\beta = 0^\circ$, $\beta = 90^\circ$ and $\beta = 140^\circ$. The BER performance is seen to have the worst characteristics for the value of $\beta = 140^\circ$ that specifically depends on the settlings of the electronic terminals and the WT. Similar to Figure 4, the same

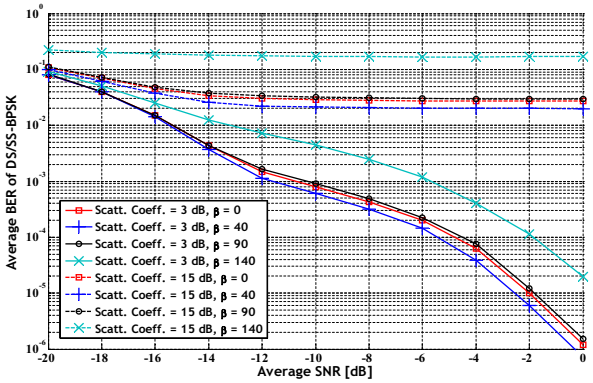

Figure 4. Variation of Average BER vs. Average SNR due to varying values of β and $\mathcal{C}_\mathcal{S}$ (For BPSK Signals and $f_c = 400$ MHz)

system setup and scattering characteristics have been examined in Figure 5 for the center frequency of $f_{c,2} = 1000$ MHz. As seen from the BER curves given in Figure 5, the variation of the performance due to the WT yaw angle, the received SNR and the scattering coefficient has the same tendency as that of the BER curves given in Figure 4, whereas the BER performance at 1000 MHz band is seen to be better than the BER performance at 400 MHz for the same system and WT scenario. For the specified center frequency of 400 MHz and 1000 MHz, and the locations of the transmitter, the receiver and the WT, the dependency of the average BER performance on the WT orientation angle (i.e., β) is depicted in Figures 6 and 7. Both figures present

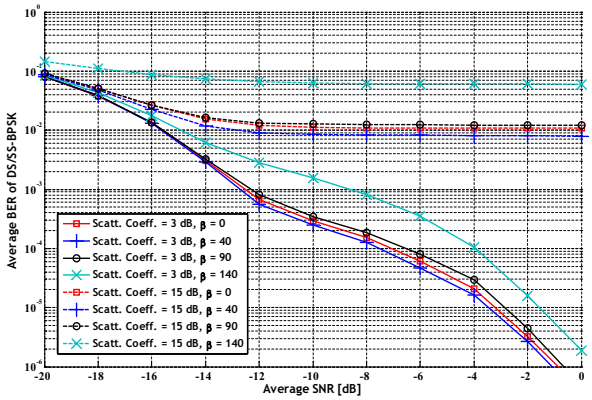

Figure 5. Variation of Average BER vs. Average SNR due to varying values of β and $\mathcal{C}_S$ (For BPSK Signals and $f_c = 1000$ MHz)

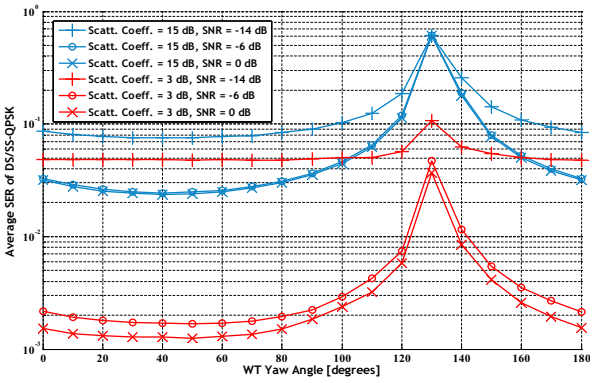

Figure 7. Variation of Average SER vs. WT Yaw Angle due to varying values of SNR and $\mathcal{C}_S$ (For QPSK Signals and $f_c = 1000$ MHz)

the average SER performances of DS/SS-QPSK signals due to varying values of $\beta = 10k$, $k = 0, 2, \ldots, 18$ for two different scattering coefficient values $\mathcal{C}_S \in \{3, 15\}$ dB and three different values of average received SNR $SNR \in \{-14, -6, 0\}$ dB. As clearly seen from both figures, the average SER performance hits its peak value at a yaw angle of approximately 130° that corresponds to the specific system and WT settlings. At the other values of β, the performance curves follow a nearly-stationary variation. The average SER performances in Figures 6 and 7 are seen to be degrading for the increasing values of $\mathcal{C}_S$. Also, for the increasing values of the received SNR, the average SER performance is clearly seen to be improved. Besides, in both figures, the enhancement provided by the increase of the received SNR value becomes more dominant for the smaller values of $\mathcal{C}_S$. For greater values of $\mathcal{C}_S$, the increase in the value of the received SNR makes negligible contribution. Note that

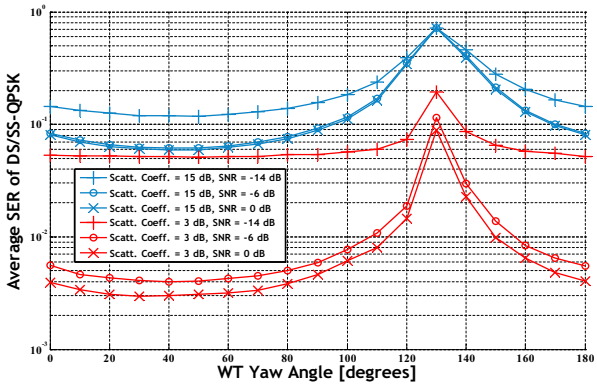

Figure 6. Variation of Average SER vs. WT Yaw Angle due to varying values of SNR and $\mathcal{C}_S$ (For QPSK Signals and $f_c = 400$ MHz)

the specific yaw angle values that are seen to face the worst SER performance is specific for the investigated system and WT locations. In order to examine the variation of this critical yaw angle value due to the variation of locations, we have considered a different system and scattering environment setup. For this purpose, Figure 8 depicts the average SER performance curves due to varying values of WT orientation angle for two different scattering coefficients $\mathcal{C}_S \in \{10, 20\}$ dB and three different values of the received SNR $SNR \in \{-14, -6, 0\}$ dB. In Figure 8, the locations of the electronic terminals and the WT have been set as $\mathbf{T} = (6000 \ -500 \ 1215)$, $\mathbf{R} = (21000 \ -500 \ 615)$ and $\mathbf{WT} = (20000 \ 0 \ 540)$, respectively. The average SER characteristics mentioned at Figures 6 and 7 have been observed in the same manner. However, the specific yaw angle that faces the worst SER performance of QPSK signals has changed to approximately 100°. Finally, Figure 9 depicts the time-dependent

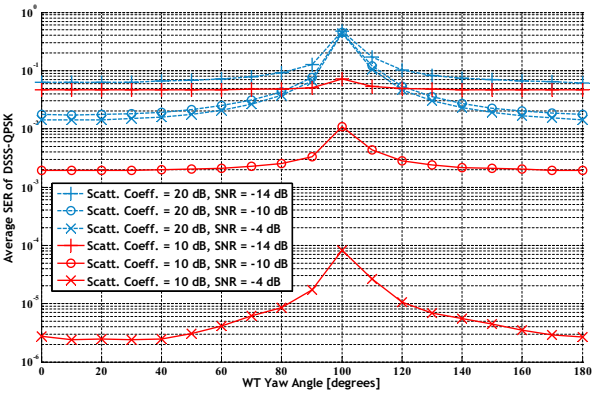

Figure 8. Variation of Average SER vs. WT Yaw Angle due to varying values of SNR, $\mathcal{C}_S$ and settling combination (For QPSK Signals and $f_c = 400$ MHz)

characteristics of the envelope of the complex scattering component (i.e., $\zeta(t)$) that has been evaluated by numerical integration given in (2). When considered together with the corresponding SER performance presented in Figure 8, it is clearly seen that the effect of the Doppler scattering on the error performance becomes more severe as the time span of the scattering component increases. Hence, the scattering component envelope for the WT orientation angle $\beta = 100^\circ$ has been spread through the entire duration of observation whereas the envelopes for the other two orientation angles are seen to be more localized in the time axis.

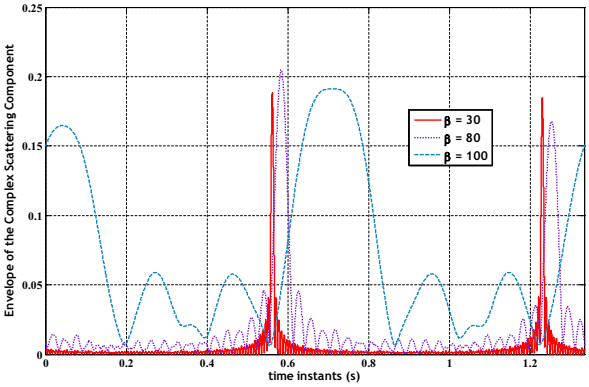

Figure 9. Variation of The Scattering Component Envelope vs. Time Instants for the scenario of Figure 8 for $\mathcal{C}_{\mathcal{S}} = 7$ dB and different values of $\beta \in \{30^\circ, 80^\circ, 100^\circ\}$

4. Conclusion

We have introduced a baseline for the investigation of WT scattering and Doppler effects on the average error performances of wireless communications systems. By defining and deriving the performance metrics in time-domain signal form, we have simulated the overall received signal that have paved the way for BER/SER performance evaluation. In addition to the proposed scattering models related to the WT scattering effects, we have considered a more causal and concrete model that has been examined for a different kind of scattering problem in [10]. By also adopting this model to WT scattering problem and including some other realistic transmission factors such as the free space path loss variation of the direct and the scattered signals, the error performance dependency on the WT orientation angle, the scattering coefficient and the terminal locations is well-investigated by useful insights provided via Monte Carlo simulations. As seen from the error performance curves, the average BER/SER performance is shown to be degrading for the increasing values of $\mathcal{C}_{\mathcal{S}}$ and the decreasing values of center frequency f_c. As expected, the increase in the average received SNR values provides direct improvements in the average error rates. As clearly seen from Figures 6, 7 and 8, the average SER performance curves hit their peak value at a yaw angle of approximately 130°, 130° and 100° that corresponds to the specific system and WT settlings. For the other values of β, the performance curves are seen to follow a nearly-stationary variation. Besides, in all figures, the enhancement provided by the increase of the received SNR value becomes more dominant for the smaller values of $\mathcal{C}_{\mathcal{S}}$. For greater values of $\mathcal{C}_{\mathcal{S}}$, the increase in the value of the received SNR makes negligible contribution on the overall error performance of the wireless communications system.

5. References

[1] R. Thresher, M. Robinson, P. Veers, "To capture the wind", *IEEE Power Energy Mag.*, vol. 5, pp. 34-46, March 2007.

[2] "Wind Farms Impact on Radar Aviation Interests", QinetiQ Ltd. Technical Report Report W/14/00614/00/REP, September 2003.

[3] "The Effects of Wind Turbine Farms on ATC Radar", Air Warfare Centre Raf Lincoln (United Kingdom), Technical Report AD Number:ADA467441, May 2005.

[4] J. Perry, and A. Biss, "Wind farm clutter mitigation in air surveilllance radar", *IEEE Aerospace and Electronic Systems Magazine*, pp. 35-40, Jul. 2007.

[5] A. Belmonte, X. Fabregas, "Impact analysis of wind turbines blockage on doppler weather radar", *in Proc. of The Fourth European Conference on Antennas and Propagation (EuCAP)*, Barcelona, Spain, 12-16 April 2010.

[6] Y. F. Lok, and A. Palevsky, "Simulation of radar signal on wind turbine", *IEEE Aerospace and Electronic Systems Magazine*, pp. 39-42, Aug. 2011.

[7] S. Aldırmaz, U. Saynak, O. Karabayır, A. F. Coşkun, H. A. Serim, Ş. Karahan, M. Ünal, B. Batı, Ö Batı, M. A. Çolak, D. Bölükbaş, K. Hocaoğlu, "Wind Turbine Effects on Radar Performance", *in Proc. of IEEE SIU 2013*, Girne, Turkish Republic of Northern Cyprus, 24-26 Apr. 2013.

[8] B. M. Isom, R. D. Palmer, G. S. Secrest, R. D. Rhoton, D. Saxion, T. L. Allmon, J. Reed, T. Crum, and R. Vogt, "Detailed Observations of Wind Turbine Clutter with Scanning Weather Radars", *American Meteorological Society*, vol. 26, pp. 894-910, 2009.

[9] C. Morlaas, M. Fares, B. Souny, "Wind Turbine Effects on VOR System Performance", *IEEE Transactions On Aerospace And Electronic Systems*, vol. 44, no. 4, pp. 1464-1476, Oct. 2008.

[10] Y. Zhang, M. G. Amin, V. Mancuso, "On the effect of rotating blades on DS/SS communication systems", *in Proc. of IEEE SSAP 2000*, pp. 682-686, PA, United States, 14-16 Aug. 2000.

[11] D. de la Vega, C. Fernández, O. Grande, I. Angulo, D. Guerra, Y. Wu, P. Angueira, J. L. Ordiales, "Software Tool for the Analysis of Potential Impact of Wind Farms on Radiocommunication Services", *in Proc. of IEEE BMSB 2011*, pp. 1-5, Germany, June 2011.

[12] I. Etayo, A. Satrustegui, M. Yabar, F. Falcone, A. Lopez, "Analysis of the frequency and time variation of radio signals scattered by a wind turbine", *in Proc. of The Fourth EuCAP*, pp. 1-3, Barcelona, Spain, 2010.

[13] D. L. Sengupta, T. B. A. Senior, "Electromagnetic interference to television reception caused by horizontal axis windmills", *IEEE Proceedings*, vol. 67, No. 8, pp. 1133-1142, Aug. 1979.

[14] I. Angulo, D. de la Vega, C. Fernández, D. Guerra, Y. Wu, P. Angueira, J. L. Ordiales, "An Empirical Comparative Study of Prediction Methods for Estimating Multipath Due to Signal Scattering From Wind Turbines on Digital TV Services", *IEEE Transactions On Broadcasting*, vol. 57, no. 2, pp. 195-203, June 2011.

[15] S. Güzelgöz, S. Yarkan, H. Arslan, "Investigation of time-selectivity of wireless channels through the use of RVC", *Elsevier Journal of Measurement*, vol. 43, no. 10, pp. 1532-1541, December 2010.

[16] R. C. Dixon, "Spread Spectrum Systems with Commercial Applications, 3rd Ed.", *John Wiley,*, 1994.